Science of the Total Environment 805 (2022) 150417

Contents lists available at ScienceDirect

Science of the Total Environment

journal homepage: www.elsevier.com/locate/scitotenv

Comprehensive characterization of industrial wastewaters using EEM fluorescence, FT-IR and ^{1}H NMR techniques

Francisco J. Rodríguez-Vidal [a,*], Beatriz Ortega-Azabache [b], Ángela González-Martínez [b], Ana Bellido-Fernández [b]

[a] Department of Chemistry, Higher Polytechnic School, University of Burgos, Av Cantabria s/n, 09006 Burgos, Spain
[b] Department of Chemistry. Faculty of Sciences, University of Burgos, Pz Misael Bañuelos s/n, 09001 Burgos, Spain

HIGHLIGHTS

- EEM fluorescence, FT-IR and ^{1}H NMR are useful techniques for wastewater analysis.
- Organic matter from industrial effluents was characterized by all three techniques.
- Pulp and paper, brewery, dairy, textile and slaughterhouse effluents were studied.
- A municipal landfill leachate was also characterized.

GRAPHICAL ABSTRACT

EEM fluorescence, FT-IR and ^{1}H NMR spectra for a textile industry effluent.

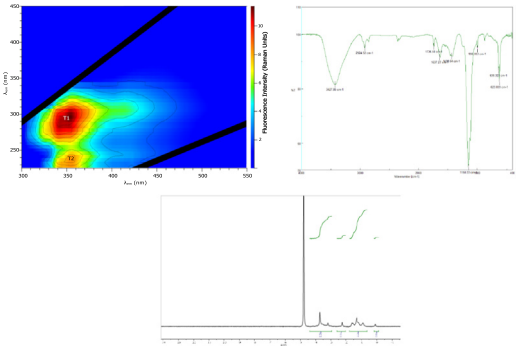

ARTICLE INFO

Article history:
Received 27 June 2021
Received in revised form 13 September 2021
Accepted 14 September 2021
Available online 17 September 2021

Editor: Damia Barcelo

Keywords:
Industrial wastewaters
Dissolved organic matter
EEM fluorescence
FT-IR
^{1}H NMR

ABSTRACT

The organic matter present in six industrial wastewaters (pulp and paper mill, brewery, textile, dairy, slaughterhouse effluents and a municipal landfill leachate) has been studied in this work using three analytical techniques: excitation-emission matrix fluorescence (EEMF), proton nuclear magnetic resonance spectroscopy (^{1}H NMR) and Fourier transform infrared spectroscopy (FTIR).

The pulp and paper mill effluent shows characteristic signals of the presence of lignins, carbohydrates and carboxylic acids, as well as sulfate, carbonate and sulfonates (coming from surfactants used in the cleaning of tanks). The main constituents of the brewery effluent are peptides and proteins coming mainly from spent yeast and diatomite filters (the presence of the latter was confirmed by Si—O bands in the FTIR spectrum). The municipal landfill leachate is characterized by the majority presence of humic substances (typical of an old landfill) and a residual presence of small peptides, amino acids and carboxylic acids. Additionally, several inorganic compounds were identified by FTIR, such as nitrate, sulfate, phosphate and cyanide ions. The textile effluent from a cotton-based industry contains carbohydrates, carboxylic acids and sulfonates, which can act as auxochromes in the textile industry. The dairy effluent comprises amino acids and small peptides coming from the biodegradation of milk and whey in addition to carbohydrates (lactose) and carboxylic acids (mainly lactic acid). The presence of tyrosine-like peaks B in the EEMF spectrum of the slaughterhouse effluent indicates the existence of small peptides and amino acids coming from the biodegradation of blood proteins. Additionally, residual glucose, fatty acids, phosphate and sulfate were also identified in this effluent.

* Corresponding author.
E-mail address: qpvito@ubu.es (F.J. Rodríguez-Vidal).

https://doi.org/10.1016/j.scitotenv.2021.150417

1. Introduction

Industrial wastewaters, even after appropriate treatment at wastewater treatment plants within the same industry, still contain a considerable amount of organic compounds remaining in the effluents. These effluents can be discharged either into municipal sewer pipes (to be treated subsequently at urban wastewater treatment plants) or directly into natural water bodies. In both cases, the inorganic and organic load of the industrial effluents can exert detrimental effects in water such as toxicity and hypoxia (Yang et al., 2015). Obviously, the composition of the effluent strongly depends on the specific type of industry (raw materials and manufacturing process) and the effectiveness of the internal wastewater treatment plant; thus, for example, the effluents from the coating industry mainly contain heavy metals whereas food industry effluents are rich in organic matter. Dissolved organic matter (DOM) in industrial effluents can comprise a great diversity of organic compounds, from simple molecules (amino acids, small peptides, simple sugars, low-molecular weight organic acids, etc.) to large macromolecules (proteins, fatty acids, carbohydrates, humic substances of supramolecular character coming mainly from the municipal water supply, etc.) (Janhom et al., 2009). In addition to the aforementioned compounds, industrial effluents usually contain residual amounts of surfactants and dispersants used in the cleaning of tanks and reactors.

Concerning DOM analysis, global parameters such as total organic carbon (TOC), biochemical oxygen demand (BOD) and chemical oxygen demand (COD) provide no information on the composition and structure of the organic compounds present in the effluent. Fluorescence has been widely used to study DOM in natural water bodies, providing in this field useful information on some structural properties of the humic substances (the main organic constituent in freshwaters), such as the aromatic character of these substances, the degree of humification and carboxylic acidity (Chen et al., 2003). It is a highly sensitive technique requiring in most cases an easy pre-treatment of the sample (usually filtration to avoid turbidity interferences). Excitation-emission matrix fluorescence (EEMF), in which a great number of emission scans are collected for a range of excitation wavelengths, is currently the most complete fluorescence technique and it can provide specific "fingerprints" for some wastewaters (Rodríguez-Vidal et al., 2020). Basically, two kinds of compounds can be identified in wastewaters by EEMF: biogenic substances (microbially derived) and humic-like substances. Protein-like substances are the biogenic substances most commonly found in waters and consist of proteins and peptides containing aromatic amino acids (mainly tryptophan and tyrosine), the main peaks being ($\lambda_{ex}/\lambda_{em}$): tryptophan-like peak T_1, tryptophan-like peak T_2, tyrosine-like peak B_1 and tyrosine-like peak B_2. Additionally, there is another biogenic peak: peak M. Humic-like substances are characterized by the following peaks: fulvic-like peak A and humic-like peak C. Unfortunately, neither carbohydrates nor lipids (common constituents of effluents) can be detected by EEMF. Infrared spectroscopy (FTIR) is especially useful for the identification of functional groups, thus allowing inferring the presence of specific organics in the sample; in complex matrices such as wastewaters, several FTIR signals can overlap into a broad band that includes the contribution of various functional groups, making it difficult the interpretation of the spectrum. ^{1}H nuclear magnetic resonance (^{1}H NMR) also provides insight into the functional groups and the aromatic character of the molecules. Similarly, ^{1}H NMR spectra of wastewaters are quite difficult to interpret due to the relatively poorly resolved resonances coming from a complex mixture of compounds. More importantly, there can be small variations in the theoretical chemical shifts caused by intermolecular interactions between the great diversity of compounds present in the effluent (Da Silva et al., 2019).

There are relatively few studies on the organic characterization of industrial wastewaters reported in the literature (urban wastewaters have been much more studied) and very few using the combination of EEMF, FTIR and ^{1}H NMR as analytical techniques. Therefore, that is precisely the aim of this work, the study of the organic composition of industrial effluents by means of all three aforementioned techniques.

2. Materials and methods

2.1. Industrial wastewaters

Six industrial effluents coming from different types of industries have been studied in this work: pulp and paper mill, brewery, textile, dairy and slaughterhouse industries along with a municipal landfill leachate. All of the industries are located at the industrial park of Burgos (Spain) and effluent samples were provided by the industry staff. Samples were filtered and refrigerated upon arrival at our laboratory. A part of the sample was freeze dried, placed into airtight glass bottles and stored in a desiccator for FT-IR and ^{1}H NMR analyses.

2.2. Excitation-emission matrix fluorescence (EEMF)

Fluorescence spectra were recorded with a spectrofluorometer (Varian Cary Eclipse) at ambient temperature (20-22 °C) using a 1-cm cuvette. The instrument settings were the following: excitation wavelength range: 220-450 nm (step 5 nm), emission wavelength range: 350-500 nm (step 1 nm), scan speed: 600 nm min^{-1}. The spectra were arranged in the form of an excitation-emission matrix (EEM) using QtiPlot software to produce two-dimensional contour plots of fluorescence intensity as a function of excitation an emission wavelengths. The spectrofluorometer was auto-zeroed before each analysis and the variation of the fluorescence intensity in triplicate experiments was less than 9%. Fluorescence intensities were normalized to Raman units (R.U) using the Raman peak of Milli-Q water at $\lambda_{ex} = 348$ nm (Yang et al., 2015). The stability of the instrument was monitored measuring the Raman emission at $\lambda_{em} = 395$ nm, which averaged 29.1 ± 1.7 intensity units ($n = 18$). Inner-filter effects were corrected by absorbance spectroscopy. The following limits of detection (in Raman Units: RU) have been estimated for the EEM fluorescence peaks found in this study: peak A: 0.071 RU, peak C: 0.015 RU, peak T1: 0.026 RU, peak T2: 0.034 RU, peak B1: 0.062 RU, peak B2: 0.092 RU, peak M: 0.053 RU. Table 1 shows the main peaks identified in the effluents (location coordinates and fluorescence intensity).

2.3. Infrared analysis

The FT-IR spectra of the powdered effluents (approximately 5% in KBr) were recorded between 400 and 4000 cm^{-1} with a spectrophotometer (Nicolet Impact 410). Accurate weighing of the sample was not required since the purpose of this work was to perform qualitative analyses, not quantitative comparisons.

2.4. ^{1}H nuclear magnetic resonance analysis

The ^{1}H NMR spectra of the powdered effluents were recorded in a Varian Mercury 300 MHz spectrometer. Approximately 5 mg of effluent powder was added to 0.5 mL deuterium oxide (D_2O) in a 10 mm NMR tube. The signal for D_2O was used as reference and set to 4.7 ppm chemical shift. The spectral window was 5000 Hz, 45° pulse angle and an acquisition time of 1.2 s/scan. Usually, 100 scans were accumulated to obtain a satisfactory signal-to-noise ratio. Accurate weighing of the sample was not required since the purpose of this work was to perform qualitative analyses, not quantitative comparisons.

3. Results

3.1. Pulp and paper mill wastewater

Pulp and paper mill effluents have a high organic load mostly composed of lignin and cellulose derivatives coming from chemical pulping

Table 1
Main EEM fluorescence peaks identified in the effluents.

Industrial category	Peak A	Peak C	Peak T_1	Peak T_2	Peak B_1	Peak B_2	Peak M
Pulp and paper	230/423 (2.81)	–	275/350 3.63)	230/360 (3.92)	–	–	305/415 (4.31)
Brewery	230/420 (1.09)	335/425 (1.42)	285/350 (2.24)	230/350 (2.21)	–	–	–
Landfill leachate	245/440 (5.93)	345/430 (17.21)	–	–	–	–	–
Textile	–	–	290/355 (10.82)	235/355 (8.15)	–	–	–
Dairy	–	325/420 (2.46)	280/355 (2.92)	225/360 (4.74)	–	–	–
Slaughterhouse	–	–	275/355 (10.20)	225/360 (8.73)	275/310 (9.62)	230/310 (7.33)	–

Peak description: λ_{ex} / λ_{em} (fluorescence intensity). λ in nm, fluorescence intensity in Raman units (RU).

processes (Carvalho et al., 2008; Duarte et al., 2003; Lal and Garg, 2017), even though up to 250 organic compounds have been identified in these effluents including phenolic compounds, carbohydrates, resin acids, terpenes, tannins, several carboxylic acids and some surfactants coming from the cleaning of tanks (Baker, 2002; Carvalho et al., 2020; Chi et al., 2018; Jaafarzadeh et al., 2017; Kaur et al., 2019; Sonkar et al., 2019; Sudarshan et al., 2016). Additionally, pulp and paper industry generates huge wastewater volumes, typically between 10 and 60 m^3 of effluent per ton of paper produced (Ciputra et al., 2010; Jaria et al., 2017).

Fig. 1.a shows the EEMF spectrum for the pulp and paper effluent and the main peaks identified are described in Table 1 (peak coordinates and fluorescence intensity). The most intense fluorescence corresponds to peak M (305/415 nm), followed by protein-like peak T_2 (230/360 nm). Peak M could be attributed to biogenic material released by microorganisms from the biological treatment of the factory wastewater treatment plant. Some authors (Baker, 2002) also suggest the contribution of whitening agents and optical brighteners used in pulp mill processes to peak M fluorescence. Other authors (Cawley et al., 2012; Ciputra et al., 2010; Muller et al., 2011) indicate that many lignin degradation compounds can also contribute to peak M, such as lignin sulfonates and lignosulfonic acid. Additionally, the aforementioned lignin derivatives have also been reported to contribute to protein-like peaks T fluorescence (Beggs and Summers, 2011; Carvalho et al., 2008; Duarte et al., 2003; Santos et al., 2000). Unfortunately, carbohydrates cannot be detected in the sample by EEMF.

The FTIR spectrum for this effluent is shown in Fig. 2.a. The typical, broad band centered at 3400 cm^{-1} can be assigned to alcoholic hydroxyl groups involved in hydrogen bonds (associated O—H stretch) coming from lignins and carbohydrates, mainly hemicellulose (Lal and Garg, 2017; Moradi et al., 2020; Sonkar et al., 2019). The weak and sharp bands at 2978 and 2933 cm^{-1} correspond to asymmetric C—H stretch of methyl and methylene groups respectively whereas the two minor bands between 2815 and 2850 cm^{-1} are assigned to symmetric C—H stretch of both CH_3 and CH_2 groups, including the C—H vibration in methoxyl groups (-OCH_3) which are abundant in lignin molecules (Behin and Sadeghi, 2016; Outeiriño et al., 2019; Simpson et al., 2004). The broad and intense band at 1558 cm^{-1} may correspond to two overlapped contributions: one of them would be the C═C stretch of aromatic rings in lignins (Behin and Sadeghi, 2016; Chi et al., 2018; Kaur et al., 2019; Outeiriño et al., 2019; Sonkar et al., 2019), especially syringil and guaiacyl units, which are well-known constituents of lignin (Carvalho et al., 2008). The other overlapped band can be attributed to the asymmetric stretch of carboxylate ion (COO^-): carboxylic groups originate during lignin degradation (Huang et al., 2019; Simpson et al., 2004), which are in the salt form since the pH of the pulp mill effluent is markedly basic (Duarte et al., 2003; Lal and Garg, 2017). Several functional groups can contribute to the broad band at 1421 cm^{-1} as well: the symmetric stretch of carboxylate ion COO^- (Abdulla et al., 2010; Rodríguez et al., 2016; Yang et al., 2015), C—H bending vibration of methyl, methylene and methoxyl groups in lignins (Kaur et al., 2019; Lal and Garg, 2017; Moradi et al., 2020; Rodríguez et al., 2016; Sonkar et al., 2019) and OH in plane bending in cellulose, hemicelluloses and lignins (Outeiriño et al., 2019). The band at 1299 cm^{-1} can be assigned to the aromatic C-O-C aliphatic stretch in ethers within the lignin macromolecule (Pretsch et al., 2009; Santos et al., 2009) and those at 1129 and 1020 cm^{-1} are characteristic of C—O stretch in alcohols and ethers from hemicelluloses and lignins (Kaur et al., 2019; Lal and Garg, 2017; Moradi et al., 2020; Outeiriño et al., 2019; Sonkar et al., 2019). Sulfonates coming from the breakdown of surfactants used in the cleaning of tanks can also contribute to the two latter bands (Chen et al., 2003; Zheng et al., 2014). Finally, the band at 667 cm^{-1} can be attributed to the S—O bond in sulfates and the band at 861 cm^{-1} can be assigned to carbonates (Jaria et al., 2017; Lal and Garg, 2017; Shouliang et al., 2008; Yang et al., 2015), both chemicals used in the pulp mill process.

Fig. 3.a shows the ^1H NMR spectrum for the pulp mill effluent. The chemical shift (δ) at 4.7 ppm corresponds to the solvent signal (D_2O). The signal at 0.9 ppm is typical of terminal -CH_3 protons (Abdulla et al., 2013; Goswami et al., 2019) and that at around 2.2 ppm can be assigned to methyl protons of the acetate functional group (CH_3COO^-) (Abdulla et al., 2013; Santos et al., 2009; Zhu et al., 2015), which is in accordance with the carboxyl groups identified by FTIR. The chemical shifts at 1.7 and 1.9 ppm can be attributed to methylene groups (Dignac et al., 2000) and the signal at 1.15 ppm might correspond to either protons in methyl groups α to hydroxy functions (Dignac et al., 2000) or methylene groups (Abdulla et al., 2013; Gonsior et al., 2011; Goswami et al., 2019; Sethupathy and Sivashanmugam, 2018). The weak band centered at around 3.5 ppm is characteristic of protons associated with oxygen-containing functional groups and is typical of carbohydrates and alcohols (Abdulla et al., 2013; Kang et al., 2002; Navalon et al., 2011), which is in line with the main organic composition assigned to this effluent, hemicellulose and lignins respectively. The other weak band at 3.85 ppm can be assigned to methoxyl groups (-OCH_3) (Gonsior et al., 2011; Zhu et al., 2015), which are abundant in the lignin structure as mentioned earlier. It is interesting to note the absence of signal for aromatic protons when aromatic rings are actually constituents of lignin structure. This fact may be explained by two reasons: the sample used in the measurement may not have been concentrated enough and lignin aromatic rings might show a high degree of substitution, resulting in a little proportion of aromatic protons. The latter explanation can be supported by the majority presence of aliphatic resonances (0.9 - 2.2 ppm) and the weak bands between 680 and 900 cm^{-1} present in the FTIR spectrum, which are characteristic of aromatic rings with a high degree of substitution (Pretsch et al., 2009). Additionally, some lignins with a very low content in syringyl units (such as those coming from pinewood) have been proven to show no aromatic proton signal (Simpson et al., 2004).

3.2. Brewery wastewater

Brewery wastewater is characterized by a high organic load, BOD and COD ranging from 2000 up to 15,000 mg O_2/L (Weathers, 1995). Beer is a fermented alcoholic beverage and in the fermentation process, yeast converts sugars (coming mainly from malt) into ethanol, carbon dioxide and other organic acids such as acetic, malic and pyruvic acids (Da Silva et al., 2019). In addition to the aforementioned compounds brewery effluents can also contain proteins, lipids and other polysaccharides (chitins, glucans, mannans,

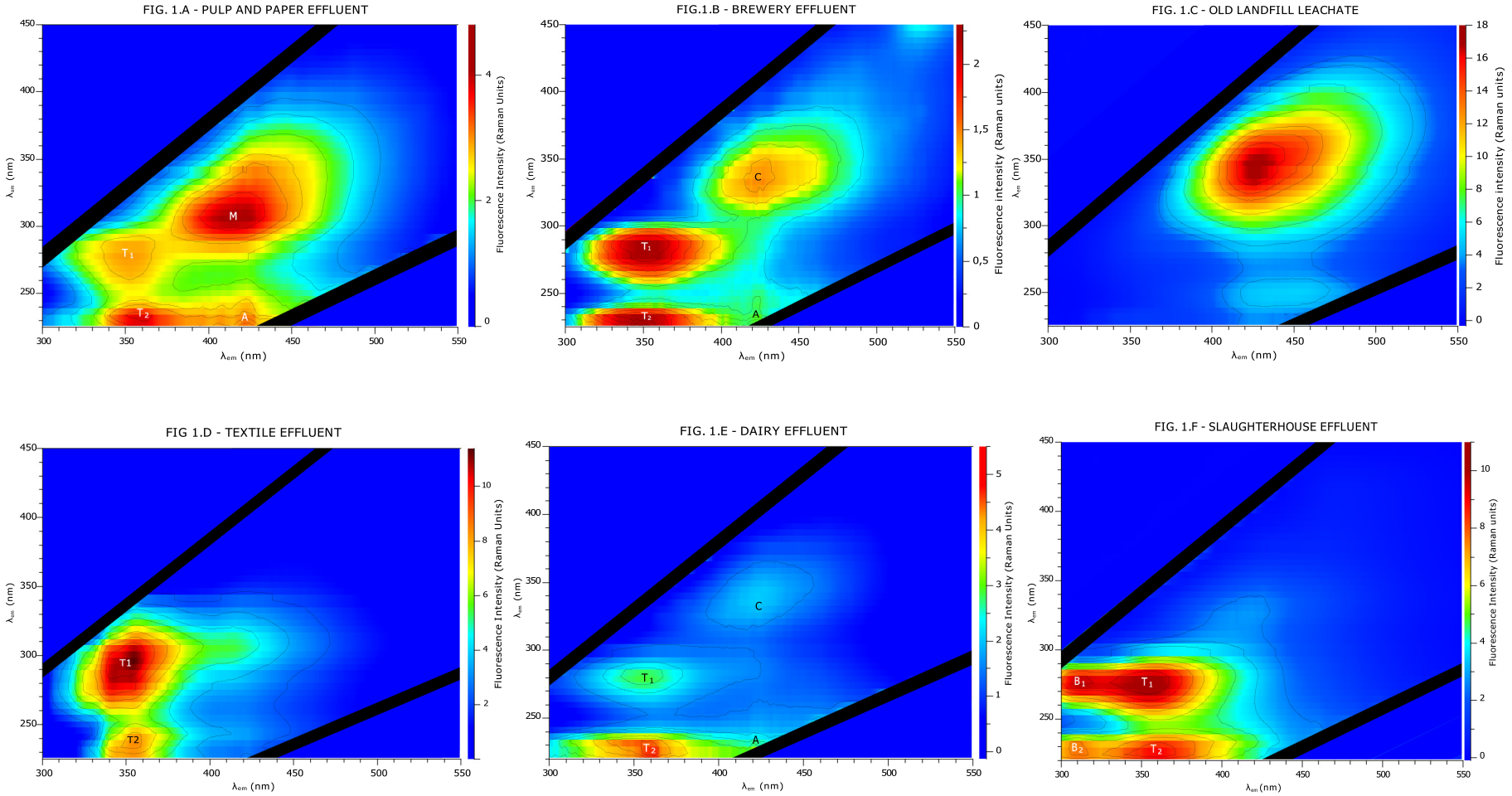

Fig. 1. EEM Fluorescence spectra for industrial effluents. A: pulp and mill paper industry, B: brewery industry, C: municipal landfill leachate, D: textile industry, E: dairy industry, F: slaughterhouse industry.

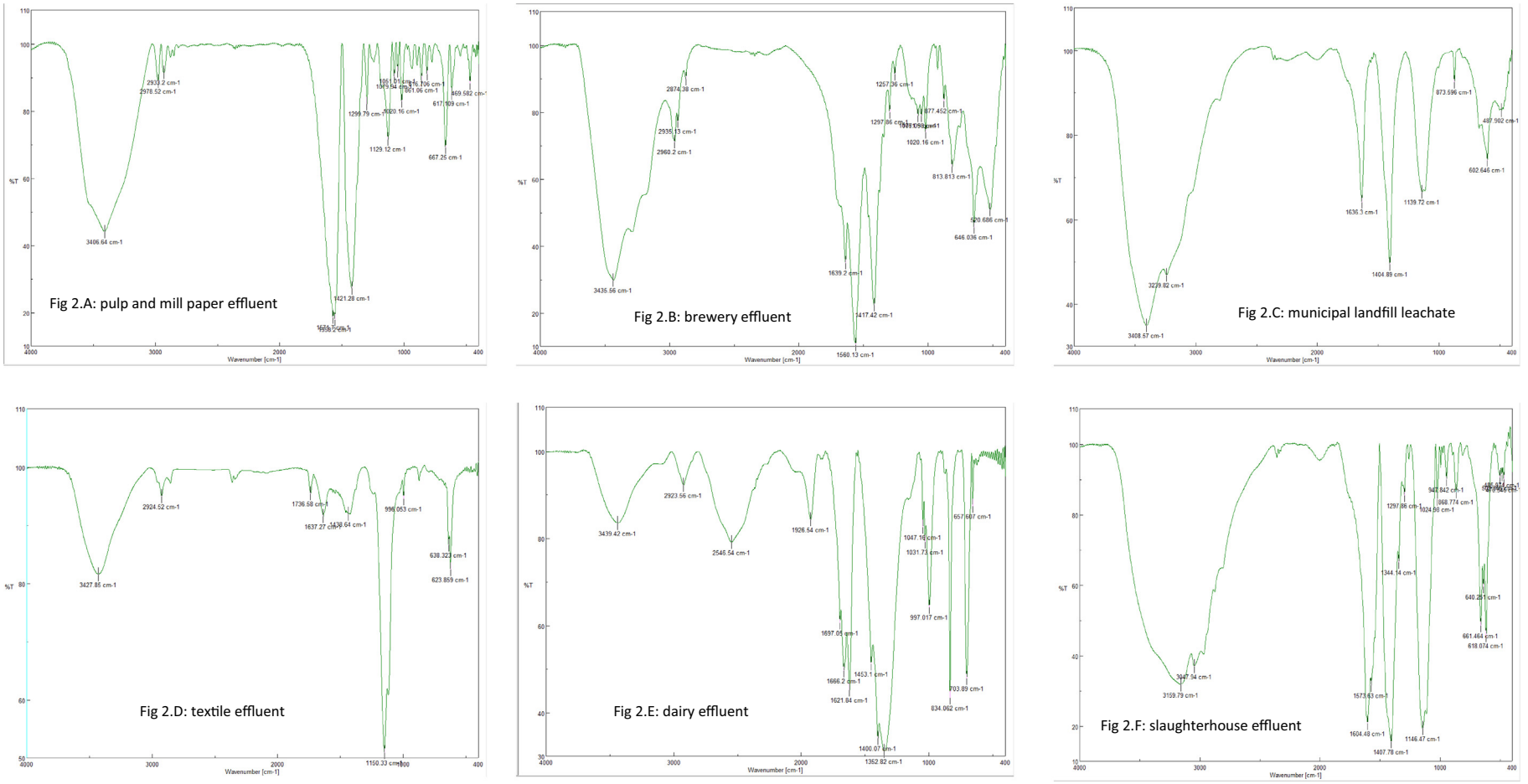

Fig. 2. FT-IR spectra for industrial effluents. A: pulp and mill paper industry, B: brewery industry, C: municipal landfill leachate, D: textile industry, E: dairy industry, F: slaughterhouse industry.

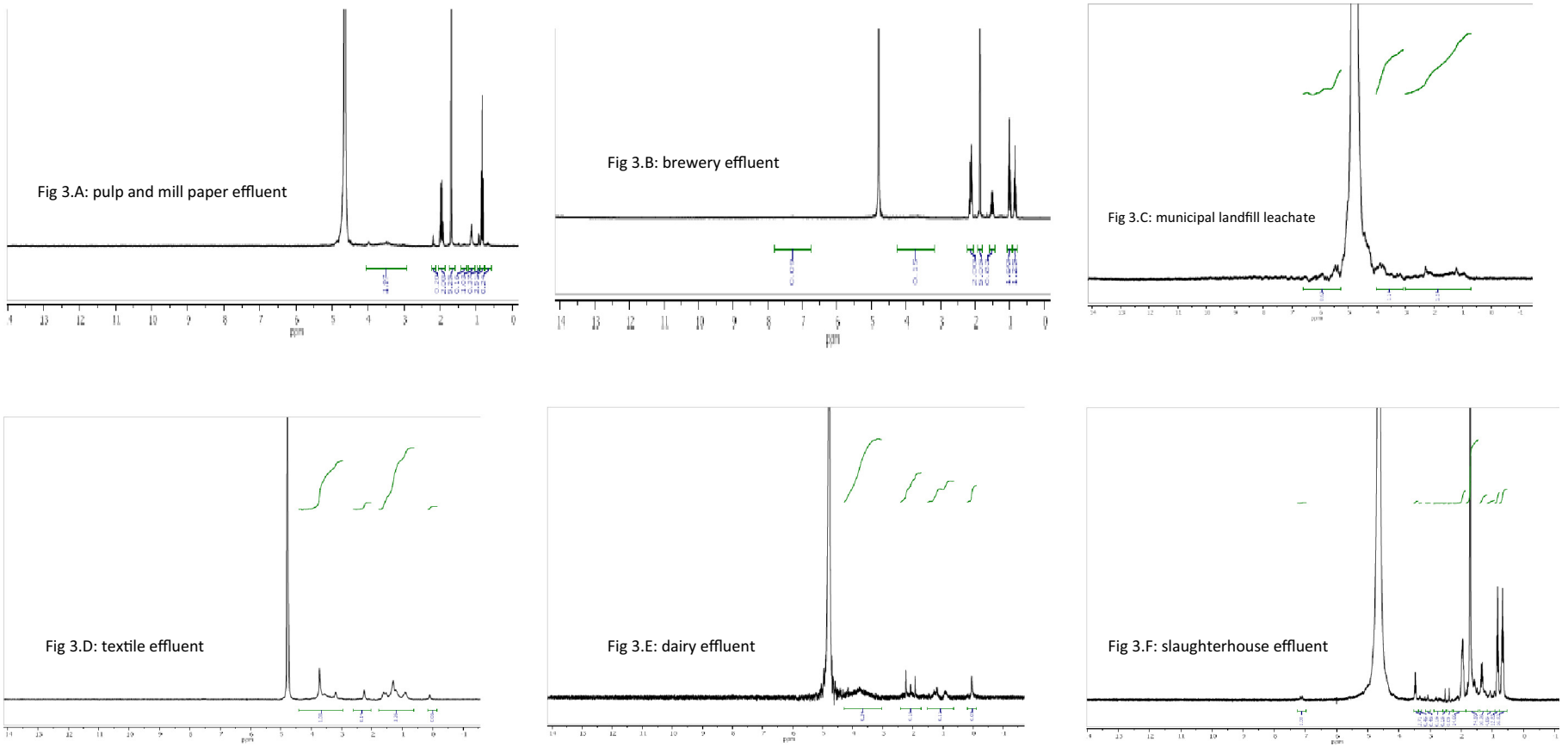

Fig. 3. ^{1}H NMR spectra for industrial effluents. A: pulp and mill paper industry, B: brewery industry, C: municipal landfill leachate, D: textile industry, E: dairy industry, F: slaughterhouse industry.

etc.) coming from the cell walls of spent yeast, specifically *Saccharomyces cerevisiae* (Stafussa et al., 2016; Tonk et al., 2015).

As seen in Fig. 1.b, the EEMF spectrum for the brewery effluent is characterized by the dominant presence of protein-like peaks T1 (285/350 nm) and T_2 (230/350 nm), a fact that clearly reflects the existence of protein moieties coming from spent yeast cells (Cooper et al., 2019), as was commented on earlier. As was mentioned in the previous Section, carbohydrates (a possible constituent of this type of wastewater) cannot be detected by EEMF.

Fig. 2.b depicts the FTIR spectrum for the brewery effluent. Several bands in the spectrum confirm the presence of proteins in the sample by this technique too: the strong broad band centered at 3435 cm^{-1} (Silbir and Goksongur, 2019; Stafussa et al., 2016) along with the two shoulder-type bands at 3200 and 3300 cm^{-1} correspond to N—H stretch in proteins and peptides, which is usually present in the form of multiplet (Pretsch et al., 2009; Tonk et al., 2015). Additionally, the bands at 1639 cm^{-1} (C═O stretch: amide I band), 1560 cm^{-1} (N-C═O stretch: amide II band) and 1257 cm^{-1} (C—N stretch: amide III band) are also characteristic of polypeptides and proteins (Navalon et al., 2011; Pretsch et al., 2009; Smidt and Meissl, 2007; Stafussa et al., 2016; Tonk et al., 2015; Yang et al., 2015). In fact, this FTIR spectrum is quite similar to that reported by Stafussa for *Saccharomyces cerevisiae* yeast (Stafussa et al., 2016). The presence of carbohydrates cannot be clearly identified in this case: they may contribute to the broad band at 3435 cm^{-1} as well (O—H stretch) and the weak bands at 1297, 1257 and 1077 might also be attributed to polysaccharides (Pretsch et al., 2009; Smidt and Meissl, 2007). In any case, the presence of carbohydrates would be residual given the little absorbance of the latter bands. Similarly, the presence of carboxylic acids (in the form of carboxylate ion, given the basic pH of this effluent) is not clear either in the spectrum: the bands at 1560 and 1417 cm^{-1} might also include the contribution of the asymmetric and symmetric COO^- stretch, respectively. The bands at 2960, 2935, 2874 and 1417 cm^{-1} correspond to $-CH_2$ and $-CH_3$ stretch that might be assigned to alkyl chains in lipids coming from spent yeast membranes (Stafussa et al., 2016; Tonk et al., 2015). There are several bands that might be attributed to the Si—O stretch coming from diatomites, such as those at 1051, 1020, 813, 646 and 520 cm^{-1} (Chi et al., 2018; Chu et al., 2016; Dignac et al., 2000; Gong et al., 2019; Ma et al., 2020; Öncü-Kaya et al., 2017; Sharma et al., 2019; Smidt and Meissl, 2007; Yang et al., 2015). Diatomite, also called "kieselguhr", is a widely-used material applied as a filter aid in the brewing industry due to its high porosity and adsorption capacity (Ma et al., 2020) and it is composed of fossilized remains of unicellular organisms such as diatoms, sponges or radiolaria. Additionally, brewery spent diatomite contains a considerable amount of proteins, which is another source of organic nitrogen to this effluent (Gong et al., 2019). Finally, the bands at 1051 and 1020 cm^{-1} could also include the contribution of sulfonate groups coming from the breakdown of surfactants used in the cleaning of tanks (Chen et al., 2003; Pernet-Coudrier et al., 2008; Smidt and Meissl, 2007; Zheng et al., 2014).

The ^1H NMR spectrum for the brewery effluent is shown in Fig. 2.c. The two signals at 0.85 and 1.0 ppm correspond to terminal methyl protons in alkyl chains of lipids/fatty acids or peptides (Gonsior et al., 2011; Goswami et al., 2019; Pretsch et al., 2009). The bands at 1.5 and 1.8 ppm can be assigned to methylene protons in lipids and peptides (Dignac et al., 2000; Goswami et al., 2019; Kumar et al., 2015; Sethupathy and Sivashanmugam, 2018; Tonk et al., 2015). The signal at 2.15 ppm might be attributed to aliphatic protons linked to carbon atoms adjacent to C═O functions, such as in carbonyl and carboxyl groups from peptides and carboxylic acids, respectively (Abdulla et al., 2013; Dignac et al., 2000; Kang et al., 2002; Gonsior et al., 2011; Goswami et al., 2019; Navalon et al., 2011; Santos et al., 2009) and the signal at 2.3 ppm has been assigned to pyruvic acid in the literature (Da Silva et al., 2019). Finally, the weak signals in the range 3.3–3.9 ppm could correspond to ethanol and carbohydrates residues, such as malt (Da Silva et al., 2019; Dignac et al., 2000; Pretsch et al., 2009).

3.3. Municipal landfill leachate

Landfill leachates are a highly complex matrix containing inorganic constituents (nitrates, sulfates, phosphates, carbonates, heavy metals, etc.), a great variety of natural organic compounds (humic substances, peptides, carbohydrates, fatty acids, etc.), xenobiotic organic compounds (chlorinated aliphatics, polycyclic aromatic hydrocarbons, polybrominated diphenyl ethers, phenols, plasticizers, pharmaceuticals, etc.) and microorganisms (Baker and Curry, 2004; Ma et al., 2018; Rodríguez-Vidal et al., 2020; Xu et al., 2017; Zhang et al., 2013). The composition of leachates strongly depends on landfill age: young leachates (landfill <5 years) still contain labile compounds (proteins, polysaccharides) whereas old leachates (landfill >10 years) are mainly composed of humic substances, which are high-molecular-weight organic matter stabilized through humification processes (Chen et al., 2019; He et al., 2013; Ji et al., 2017; Li et al., 2010; Lu et al., 2009; Sun et al., 2018; Wang et al., 2016).

The EEMF spectrum for an old landfill leachate is depicted in Fig. 1.c. The spectrum shows a dual fluorescence peak (245/440 nm and 345/430 nm) corresponding to humic material of both fulvic- and humic-like character, which confirms that humic substances are the dominant organic matter in the leachate (Li et al., 2016; Liu et al., 2020; Lu et al., 2009; Shouliang et al., 2008; Xu et al., 2017; Wang et al., 2020). Other authors also report the contribution of lignocellulose-like compounds and melanoidin-like compounds to peak C fluorescence in landfill leachates (Zegzouti et al., 2020). There are no trace of protein-like peaks, which is in accordance with the landfill age (Xi et al., 2008). No more information can be inferred from the spectrum.

Fig. 2.c. shows the FTIR spectrum for this leachate. Humic substances are macromolecules of acidic character with a high content in carboxylic and phenolic groups. Due to the basic pH of the old leachate (around 8.5) (Cheng et al., 2021) carboxylic groups are mostly deprotonated, which could be indicated by the bands at 1636 and 1404 cm^{-1} that have been attributed in the literature to the asymmetric and symmetric stretch of carboxylate ion (COO^-) respectively in leachate humic substances (Abdulla et al., 2010; Ferraz et al., 2016; Öncü-Kaya et al., 2017; Shouliang et al., 2008; Wang et al., 2017). The typical, broad band centered at 3408 cm^{-1} can be assigned to intermolecular O—H stretch or H-bonded OH groups coming from phenolic groups in humic substances (Ai et al., 2019; Liu et al., 2018; Tahiri et al., 2016; Yang et al., 2015). Old landfill leachates are rich in amino acids and small peptides due to the hydrolysis of large proteins (Oloibiri et al., 2017; Renou et al., 2008), therefore the latter band at 3408 cm^{-1} can also contain the contribution of the N—H stretch (Hur et al., 2014; Liu et al., 2015; Tahiri et al., 2016). This fact can be confirmed by the two shoulders at 3239 and 3050 cm^{-1} typical of N—H stretch in peptides (amide bond) (Pretsch et al., 2009; Tonk et al., 2015), as was mentioned in Section 3.2. Other bands in the leachate spectrum that can be attributed to peptides are those at 1636 cm^{-1} (C═O stretch: amide I band) (Hur et al., 2014; Liu et al., 2015; Pretsch et al., 2009) and at 1404 cm^{-1} (C—N stretch) (Ai et al., 2019; Yang et al., 2015). The width of the bands at 1636, 1404 and 1139 cm^{-1} clearly suggests the contribution of several overlapped signals. The band at 1636 cm^{-1} may include the contributions of carboxylate ion (humic substances), amide I band (small peptides) and aromatic C═C bond in humic substances (Fan et al., 2006; Ferraz et al., 2016; Jin et al., 2019; Karimipourfard et al., 2020; Liu et al., 2018; Santos et al., 2009). The band at 1404 cm^{-1} can be due to carboxylate ion (humic substances), O—H deformation and C—O stretch of phenolic groups (humic substances) (Guo et al., 2012; Santos et al., 2009; Tahiri et al., 2016; Xiaoli et al., 2013), C—H deformation of alkyl CH_3 and CH_2 (humic substances and peptides) (Karimipourfard et al., 2020; Liu et al., 2018), C—N stretch (peptides) (Ai et al., 2019; Karthikeyan et al., 2011; Yang et al., 2015) and N—O stretch in nitrate (NO_3^-) (Rodríguez et al., 2016; Shouliang et al., 2008; Smidt and Meissl, 2007; Wang et al., 2017). The band at 1139 cm^{-1} can be attributed to both S—O stretch in sulfate (SO_4^{2-}) (Lenz et al.,

2016; Smidt and Meissl, 2007; Yang et al., 2015) and C—O stretch in phenols (humic substances) (Smidt and Meissl, 2007). The sharp weak band at 873 cm^{-1} can be assigned to either C—O out-of-plane in carbonate (CO_3^{2-}) (Shouliang et al., 2008; Yang et al., 2015) or C—H bending in aromatic rings with a high degree of substitution (Jin et al., 2019; Karimipourfard et al., 2020; Smidt and Meissl, 2007). Finally, the broad band at 602 cm-1 can include the contribution of sulfate (Ai et al., 2019; Lal and Garg, 2017; Liu et al., 2018; Yang et al., 2015), phosphate (Wang et al., 2016, 2017), silicate (Tahiri et al., 2016) and alkyl-halides (C-X stretch) from xenobiotic compounds (Hur et al., 2014). The broad, weak shoulder centered at 2050 cm^{-1} has been reported in the literature to correspond to cyanide ions (CN^-) in leachates (Silva et al., 2019).

The leachate ^1H NMR spectrum is shown in Fig. 3.c. Typically, the signals at 1.0 and 1.2 ppm correspond to aliphatic methyl and methylene groups, respectively. The chemical shift at 2.3 ppm can be assigned to protons on carbon in α position to carboxyl groups, which might confirm the presence of carboxylic acids (in the salt form given the basic pH of the leachate). The two poorly resolved bands between 3 and 4 ppm cannot be attributed to polysaccharides in this case since these compounds are not expected in old landfill leachates due to their high biodegradability. These signals might be assigned to methine and methylene protons in small peptides and amino acids (Navalon et al., 2011; Pretsch et al., 2009; Tahiri et al., 2016), the presence of which was also identified by FT-IR. The weak bands between 5.5 and 6.5 ppm could correspond to the N—H proton in the peptide bond (Pretsch et al., 2009). Even though humic substances are aromatic macromolecules, it is interesting to note that there are very weak resonances in the aromatic region (6.5–9 ppm). Similar cases have been reported in the literature (Rodríguez et al., 2016; Tahiri et al., 2016) and this fact might be due to a high degree of substitution in the aromatic rings within the humic macromolecule.

3.4. Textile industry wastewater

Textile industry produces huge volumes of wastewater due to its high consumption of water through all stages within the productive process: sizing, scouring, bleaching, mercerizing, dyeing, printing and finishing (Li et al., 2015; Sharma et al., 2019; Yin et al., 2018). These wastewaters are characterized by high COD (Chemical Oxygen Demand), color, turbidity and temperature (Fan et al., 2014; Jain et al., 2014; Yurtsever et al., 2016). The organic compounds present in textile industry wastewaters depend on the raw materials used in the process (cotton, PET, nylon, etc.) and the use of specific chemicals, such as sizing agents (polyvinyl alcohol, carboxymethyl cellulose, starch), surfactants, dispersants and dyestuff (Cheng et al., 2020; Wang et al., 2019). The effluent studied in this Section corresponds to a textile industry manufacturing cotton-based clothes.

The EEMF spectrum for the textile effluent is depicted in Fig. 1.d and it shows the predominant presence of protein-like peaks T, which is in accordance with most of the literature (Cheng et al., 2018, 2020; Liu et al., 2019; Wang et al., 2019). Even though a part of the fluorescence in this region can be due to SMP (Soluble Microbial Products) released by microorganisms during the biological stage at the internal wastewater treatment plant (Cheng et al., 2018; Yin et al., 2017; Yurtsever et al., 2016), in the specific case of textile effluents this fluorescence can also correspond to the incomplete degradation products of some dispersants and surfactants used in these industries, which are highly water-soluble and are not completely degraded during the biological treatment (Cheng et al., 2018, 2020). Other studies attribute the protein-like fluorescence in textile industry effluents to metabolites of azo dyes also generated at the biological stage of the wastewater treatment (Cheng et al., 2020; Li et al., 2015; Wang et al., 2019; Wu et al., 2016). Unfortunately, the presence of carbohydrate residues coming from cellulose fibers (cotton) cannot be detected by EEMF.

Fig. 2.d shows the textile effluent FTIR spectrum. Since the industry studied here works with cotton-based fabrics (cotton is roughly composed of 94% cellulose) the presence of carbohydrate-related bands is expected in the spectrum. Indeed, the bands at 3427 cm^{-1} (O—H stretch), at 1438 cm^{-1} (C-O-H band) and at 1150 cm^{-1} (C—O stretch, the most intense band) can be assigned to carbohydrates (Balapure et al., 2016; Meenatchisundaram et al., 2014; Pretsch et al., 2009). The weak band at 1736 cm^{-1} might indicate a minimum presence of carboxylic acids in the acidic form (since the pH of this effluent is almost neutral: pH = 7.5), which can be used as auxochromes to intensify color and improve the binding capacity of dyes onto the textile material (Balapure et al., 2016; Fan et al., 2014). The presence of sulfonates, used as auxochromes as well but also coming from surfactants and detergents during the cleaning of tanks, can be inferred from the bands at 1150 and 996 cm^{-1} (Balapure et al., 2015, 2016; Chen et al., 2003; Zheng et al., 2014). Finally, the bands at 2924 cm^{-1} (methyl and methylene groups) and at 1438 cm^{-1} (C—H stretch) correspond to aliphatic chains (Balapure et al., 2016; Meenatchisundaram et al., 2014) and the band at 623 cm^{-1} can be attributed to sulfate (Ai et al., 2019; Lal and Garg, 2017; Liu et al., 2018; Yang et al., 2015). Our FTIR spectrum has many features in common with some other FTIR spectra reported in the literature for textile effluents (Jain et al., 2014; Karthikeyan et al., 2011).

The ^1H NMR spectrum for the textile effluent is shown in Fig. 3.d. The most intense signal in the spectrum at 3.7 ppm is typically assigned to carbohydrate residues (Abdulla et al., 2013; Dignac et al., 2000; Kang et al., 2002; Tahiri et al., 2016), the presence of which was confirmed by FTIR. The resonance at 0.9 ppm corresponds to methyl protons and the poorly resolved signals at 1.25 and 1.60 ppm are typical of methylene groups (Dignac et al., 2000; Gonsior et al., 2011; Kumar et al., 2015; Navalon et al., 2011; Sethupathy and Sivashanmugam, 2018). Finally, the chemical shift at 2.25 ppm can be attributed to protons on carbon in α position to carboxyl groups (Kang et al., 2002; Kumar et al., 2015; Santos et al., 2009), since the presence of a little amount of carboxylic acids has also been detected by FTIR.

3.5. Dairy industry wastewater

Dairy industry generates large volumes of wastewater with a high content in organic matter (COD, BOD) and nutrients (nitrogen and phosphorus) (Ahmad et al., 2020; Behera et al., 2019; Rabinovich et al., 2018). Since most of the oils and fats are removed through flotation techniques at the internal wastewater treatment plants, most of the remaining organic matter in the effluent is composed of milk and whey residues coming from the cleaning of tanks and reactors. These residues mainly comprise proteins such as casein (a phosphoprotein), beta-lactoglobulin and alpha-lactalbumin, lactose (carbohydrate) and lactic acid (Bi et al., 2016; Muniz et al., 2020a, 2020b; Shumilina et al., 2020; Zinadini et al., 2015).

The EEMF spectrum of the dairy effluent shown in Fig. 1-e is dominated by protein-like fluorescence, peak T2 (225/360 nm) being the prevailing one. This fluorescence is likely due to small peptides and amino acids since large proteins are expected to be partially degraded during the biological treatment at the wastewater treatment plant. Actually, some studies on dairy effluents and UF permeates support this assumption, assigning peak T1 fluorescence to tryptophan-containing proteins whereas peak T2 would correspond to tryptophan-containing amino acids and peptides (Ma and Amamcharla, 2019). A low fluorescence peak C (335/420 nm) is also present in the EEMF spectrum, but it is not likely to correspond to humic acids coming from the drinking water supply since fulvic acids (peak A) are the most abundant humic substances in natural waters. In the case of dairy wastewaters peak C fluorescence is attributed to melanoidins and lipofuscins derived from protein and sugar oxidation in thermally treated milk (Maillard reaction) (Muller et al., 2011). Our dairy effluent EEMF spectrum shows some similarities with others reported in the literature for milk and whey UF permeates (Ma and Amamcharla, 2019) and for milk beta-casein and alpha-lactalbumin (Bi et al., 2016). As was mentioned in

previous Sections, the presence of lactose or its components (glucose and galactose) cannot be detected by this technique.

Fig. 2-e shows the FTIR spectrum for the dairy effluent. The width of most bands indicates the overlapping of several signals. Concerning nitrogen-containing compounds, it is expected the presence of small peptides (peptide bond), amino acids in the form of zwitterions (the predominant form at neutral pH, which is the pH of this effluent; in the zwitterion form both carboxyl and amino groups are ionized as $-COO^-$ and $-NH_3^+$, respectively) and inorganic ammonium (NH_4^+), a major constituent of dairy wastewater too (Rabinovich et al., 2018). The typical broad band centered at 3439 cm^{-1} can be attributed to both the O—H stretch in carbohydrates (lactose) and the N—H stretch in peptides (Pretsch et al., 2009). The weak shoulder at 3100 cm^{-1} is typical of peptides (amide group) and the band at 2923 cm^{-1} is normally attributed to methyl and methylene groups but due to its unusual width it might include the contribution of the inorganic ammonium NH_4^+ stretch (Pretsch et al., 2009). The broad band at 2546 cm^{-1} and that at 1926 cm^{-1} may also correspond to the overlapped signals of both the $-NH_3^+$ stretch in amino acids (zwitterions) and the NH_4^+ stretch of inorganic ammonium (Pretsch et al., 2009). The poorly resolved band at 1697 cm^{-1} can be attributed to the carboxyl group C═O stretch (mainly lactic acid, even though some other carboxylic acids have also been found in dairy effluents, such as acetic, citric and butyric acids) (Shumilina et al., 2020), the signal at 1666 cm^{-1} can correspond to the C═O stretch of the amide group in peptides (amide I band) (Yang et al., 2015) and the nearby band at 1621 cm^{-1} may be assigned to NH_3^+ bending and COO^- stretch in amino acids in the form of zwitterions) (Pretsch et al., 2009). The width of the two overlapped bands at 1400 and 1352 cm^{-1} suggests the contribution of several signals, such as the O—H bending band of carbohydrates (lactose) (Balapure et al., 2016; Pretsch et al., 2009), the N—O stretch in nitrate (NO_3^-) which is also present in dairy wastewaters (Ahmad et al., 2020; Rodríguez et al., 2016), the C—H deformation of alkyl CH_3 and CH_2 (peptides) (Karimipourfard et al., 2020; Liu et al., 2018), the C—N stretch in peptides (Ai et al., 2019; Yang et al., 2015) and the C—O stretch in carbonate (CO_3^{2-}) (Rabinovich et al., 2018; Yang et al., 2015). The three overlapped bands at 1047, 1031 and 997 cm^{-1} can include the contribution of the C—O stretch in carbohydrates (lactose), sulfonates coming from detergents used in the cleaning of tanks and reactors (Chen et al., 2003; Zheng et al., 2014) and the P-O-P stretch in inorganic phosphate (PO_4^{3-}) (Rabinovich et al., 2018; Sales et al., 2020). Finally, the last bands at low wavenumbers correspond to inorganic compounds: the two narrow, intense bands at 834 and 703 cm^{-1} can be attributed to carbonate (CO_3^{2-}) (Rabinovich et al., 2018; Smidt and Meissl, 2007; Yang et al., 2015) and the low intensity signal at 657 cm^{-1} can be assigned to sulfate (SO_4^{2-}) (Lal and Garg, 2017; Shouliang et al., 2008; Yang et al., 2015).

The ^1H NMR spectrum for the dairy effluent is shown in Fig. 3-e. Typically, the chemical shift at 0.9 ppm corresponds to methyl protons and the poorly resolved signal at 1.25 ppm is characteristic of methylene groups (Gonsior et al., 2011; Kumar et al., 2015; Navalon et al., 2011; Sethupathy and Sivashanmugam, 2018). The three signals between 1.95 and 2.25 ppm are typical of protons on carbon in α position to carbonyl and carboxyl groups from peptides and carboxylic acids, respectively (Abdulla et al., 2013; Goswami et al., 2019; Navalon et al., 2011; Santos et al., 2009). Finally, the broad, unresolved band centered at 3.75 ppm can include the contribution of carbohydrates (lactose), lactic acid (proton on carbon in α position to both hydroxyl and carboxyl groups) and amino acids in the zwitterion form (protons on carbon in α position to both carboxylate and ammonium groups) (Pretsch et al., 2009).

3.6. Slaughterhouse wastewater

The cattle slaughter industry generates huge volumes of wastewater with a high content in organic matter (COD and BOD), mainly residual blood, animal fat and feces (Louvet et al., 2013). Most of this organic matter can be readily removed by either aerobic or anaerobic biological treatments at wastewater treatment plants (Mittal, 2006).

Fig. 1-f shows the EEMF spectrum for a cattle slaughterhouse effluent (specifically, this industry slaughters cows, calves and pigs). It can be seen that the predominant fluorescence corresponds to protein-like peaks but unlike the previous cases, tyrosine-like peaks B (B1: 275/310 nm and B2: 230/310 nm) also appear in this spectrum. Tyrosine-like peaks B are much less frequent in wastewaters than tryptophan-like peaks T because peaks B fluorescence can be quenched in high-molecular weight proteins: the energy absorbed by tyrosine is transferred to tryptophan moieties within the same protein (Bridgeman et al., 2013; Rodríguez-Vidal et al., 2020). That is why the appearance of peaks B in a sample strongly suggests the presence of small peptides and/or free amino acids (and not large proteins) in which tryptophan is absent. That makes sense in this case since the anaerobic-aerobic biological treatment at the internal wastewater treatment plant is effective enough to degrade large proteins into their smaller constituents (peptides and amino acids). It is interesting to note the high fluorescence intensity of the protein-like peaks, which is due to the high concentration of blood proteins (mainly serum albumin and hemoglobin) in these kinds of effluents (Louvet et al., 2013).

The FTIR spectrum for the cattle slaughterhouse effluent is shown in Fig. 2-f. The typically broad band centered at 3159 cm^{-1} mainly corresponds to the N—H stretch in peptides and amino acids (the shoulder at 3047 cm^{-1} is typical of peptides) (Pretsch et al., 2009; Tonk et al., 2015), even though this band can also include the contribution of glucose residues from the blood plasma (Upadhyay et al., 2020); fatty acids do not contribute to this band since they are ionized at the basic pH of this effluent (pH = 9.0). The little shoulders at 2960, 2890 and 2850 cm^{-1} mainly from fatty acids (Guleken et al., 2020; Guo et al., 2012; Zhu et al., 2015). The width of the band at 1604 cm^{-1} suggests the contribution of several overlapped signals: the C═O stretch in peptides (amide I band) (Asses et al., 2019; Fagbemi et al., 2020; Navalon et al., 2011), the carboxylate ion (COO^-) asymmetric stretch in ionized fatty acids (Lal and Garg, 2017) and the C═C stretch of aromatic rings in tryptophan and tyrosine (aromatic amino acids), which were identified by EEMF (Asses et al., 2019; Guleken et al., 2020). The poorly resolved band at 1573 cm^{-1} can be attributed to the N-C═O stretch in peptides (amide II band) (Fagbemi et al., 2020; Sales et al., 2020). The broad, intense band at 1407 cm^{-1} can also be attributed to the overlap of several signals: the carboxylate ion (COO^-) symmetric stretch in ionized fatty acids (Asses et al., 2019; Pretsch et al., 2009), the C—H bending vibration of methyl and methylene groups in alkyl chains from fatty acids (Stafussa et al., 2016; Tonk et al., 2015), the O—H in plane bending in glucose residues (Balapure et al., 2016; Sales et al., 2020) and the C—N stretch in peptides (Ai et al., 2019; Yang et al., 2015). Similarly, the band at 1146 cm^{-1} can include the contribution of sulfonates (along with the 1024 cm^{-1} band) coming from surfactants used in the cleaning of tanks (Chen et al., 2003; Zheng et al., 2014), the P═O stretch in phospholipids (Pretsch et al., 2009; Sales et al., 2020), the C—O stretch in carbohydrates (glucose) (Asses et al., 2019; Lal and Garg, 2017; Yang et al., 2015) and sulfate (SO_4^{2-}), which may originate from the oxidation of disulphide bonds (S—S) present in bovine serum albumin (this protein is rich in cysteine) (Fagbemi et al., 2020; Shouliang et al., 2008) and/or from some sulfate-containing salts used in the wastewater treatment. Other bands that can be attributed to phosphate are those at 1024, 947 and 618 cm^{-1} (Sales et al., 2020; Wang et al., 2016, 2017). Finally, the bands at 661 and 618 cm^{-1} can also be attributed to sulfate (Lal and Garg, 2017; Shouliang et al., 2008; Yang et al., 2015).

Fig. 3-f shows the ^1H NMR spectrum for the cattle slaughterhouse effluent. There are no chemical shifts characteristic of the Heme group in the downfield part of the spectrum (> 10 ppm) (Senn et al., 1984; Wójtowicz et al., 2009), therefore it can be assumed that the Heme group was degraded at the biological stage of the wastewater treatment.

The chemical shift at 1.7 ppm greatly differs in intensity from the rest of signals in the spectrum, which indicates that it is not related to them and might originate from an unidentified chemical agent or solvent used in the cleaning of tanks. Regarding the rest of signals in the spectrum, the most intense ones can be attributed to aliphatic methyl (0.7 and 0.85 ppm) and methylene (1.3 and 1.6 ppm) groups in fatty acids and lipids from blood plasma (Goswami et al., 2019; Kumar et al., 2015; Upadhyay et al., 2020), protons linked to carbon atoms adjacent to C═O functions in fatty acids and peptides (2 ppm) (Abdulla et al., 2013; Gonsior et al., 2011; Navalon et al., 2011), residual glucose (3.5 ppm) (Upadhyay et al., 2020) and aromatic rings from tyrosine and tryptophan in serum albumin peptides (7.1 ppm), the presence of which was confirmed by EEMF. It can be observed in the spectrum that there are also multiple low intensity, poorly resolved signals in the region 0.9- 4 ppm. These chemical shifts have been attributed in the literature to several amino acids (glycine, proline, glutamine, aspartate, etc.) and some organic acids (succinate, lactate, acetate, pyruvate, citrate, etc.) (Upadhyay et al., 2020).

4. Conclusions

Six industrial wastewaters (pulp and paper mill, brewery, textile, dairy and slaughterhouse effluents and a municipal landfill leachate) have been studied in this work using three analytical techniques: excitation-emission matrix fluorescence (EEMF), proton nuclear magnetic resonance spectroscopy (^{1}H NMR) and Fourier transform infrared spectroscopy (FTIR).

- Pulp and paper mill effluent: characteristic signals of the presence of lignins, carbohydrates and carboxylic acids were identified by both FTIR and ^{1}H NMR. Sulfonates (coming from surfactants used in the cleaning of tanks), sulfate and carbonate were also detected by FTIR.
- Brewery effluent: the main constituents of this effluent, identified by all the three techniques, are peptides and proteins coming mainly from spent yeast and diatomite filters (the presence of the latter was confirmed by Si—O bands in the FTIR spectrum). A residual presence of ethanol, carbohydrates and organic acids was also detected by both FTIR and ^{1}H NMR.
- Municipal landfill leachate: humic substances are the only compounds that appear in the EEMF spectrum. There is no presence of protein-like peaks, which is in accordance with the old age of the landfill studied. Traces of carboxylic and several inorganic compounds were identified by FTIR, such as nitrate, sulfate, phosphate and cyanide ions.
- Textile effluent: protein-like peaks are predominant in the EEMF spectrum. Since it is a cotton-based textile industry, the presence or carbohydrates in the effluent is confirmed by both FTIR and ^{1}H NMR, as well as a residual presence of carboxylic acids and sulfonates, which can act as auxochromes in the textile industry.
- Dairy effluent: small peptides and amino acids coming from the biodegradation of milk and whey proteins are detected by EEMF, as well as some melanoidins derived from protein and sugar oxidation in thermally treated milk. Additionally, amino acids, small peptides, carbohydrates (lactose) and carboxylic acids (mainly lactic acid) were identified by both FTIR and ^{1}H NMR.
- Slaughterhouse effluent: the presence of tyrosine-like peaks B in the EEMF spectrum indicates the existence of small peptides and amino acids in the effluent, coming from the biodegradation of blood proteins. In addition to these compounds, residual glucose and fatty acids were also identified by both FTIR and ^{1}H NMR. FTIR also allowed the detection of some inorganic ions, such as phosphate and sulfate.

Obviously, more research is needed to complete this work: more effluents from industrial facilities belonging to the categories studied in this work must be sampled and characterized in order to check these preliminary results.

CRediT authorship contribution statement

Francisco J. Rodríguez-Vidal: Conceptualization, Resources, Writing – original draft, Writing – review & editing, Visualization, Project administration. **Beatriz Ortega Azabache:** Investigation, Formal analysis, Data curation. **Ángela González Martínez:** Investigation, Formal analysis, Data curation. **Ana Bellido Fernández:** Investigation, Formal analysis, Data curation.

Declaration of competing interest

The authors declare that they have no known competing financial interests or personal relationships that could have appeared to influence the work reported in this paper.

References

Abdulla, H., Minor, E., Dias, R., Hatcher, P., 2010. Changes in the compound classes of dissolved organic matter along an estuarine transect: a study using FTIR and 13C NMR. Geochim. Cosmoschim. Acta. 74, 3815–3838.

Abdulla, H., Minor, E., Dias, R., Hatcher, P., 2013. Transformations of the chemical compositions of high molecular weight DOM along a salinity transect: using two dimensional correlation spectroscopy and principal component analysis approaches. Geochim. Cosmochim. Acta. 118, 231–246.

Ahmad, S., Kothari, R., Pathania, D., Tyagi, V., 2020. Optimization of nutrients from wastewater using RSM for augmentation of Chlorella pyrenoidosa with enhanced lipid productivity, FAME content and its quality assessment using fuel quality index. Biomass Convers. Biorefinery. 10, 495–512.

Ai, J., Wu, X., Wang, Y., Zhang, H., 2019. Treatment of landfill leachate with combined biological and chemical processes: changes in the dissolved organic matter and functional groups. Environ. Technol. 40, 2225–2231.

Asses, N., Farhat, W., Hamdi, M., Bouallagui, H., 2019. Large scale composting of poultry slaughterhouse processing waste: microbial removal and agricultural biofertilizer application. Process Saf. Environ. Protect. 124, 128–136.

Baker, A., 2002. Fluorescence excitation-emission matrix characterization of river waters impacted by a tissue mill effluent. Environ. Sci. Technol. 36, 1377–1382.

Baker, A., Curry, M., 2004. Fluorescence of leachates from three contrasting landfills. Water Res. 38, 2605–2613.

Balapure, K., Bhatt, N., Madamwar, D., 2015. Mineralization of reactive azo dyes present in simulated textile wastewater using down flow microaerophilic fixed film biorreactor. Biores. Technol. 175, 1–7.

Balapure, K., Jain, K., Bhatt, N., Madamwar, D., 2016. Exploring bioremediation strategies to enhance the mineralization of textile industrial wastewater through sequential anaerobic-microaerophilic process. Int. Biodeterior. Biodegrad. 106, 97–105.

Beggs, K.M.H., Summers, R.S., 2011. Character and chlorine reactivity of dissolved organic matter from a mountain pine beetle impacted watershed. Environ. Sci. Technol. 45, 5717–5724.

Behera, A.R., Dutta, K., Verma, P., Daverey, A., Sahoo, D.K., 2019. High lipid accumulating bacteria isolated from dairy effluent scum grown on dairy wastewater as potential biodiesel feedstock. J. Environ. Manag. 252, 109686.

Behin, J., Sadeghi, N., 2016. Utilization of waste lignin to prepare controlled-slow release urea. Int. J. Recycl. Org. Waste Agric. 5, 289–299.

Bi, H., Tang, L., Gao, X., Jia, J., Lv, H., 2016. Spectroscopic analysis on the binding interaction between tetracycline hydrochloride and bovine proteins beta-casein, alpha-lactalbumin. J. Luminiscence 178, 72–83.

Bridgeman, J., Baker, A., Carliell, C., Carstea, E., 2013. Determination of changes in wastewater quality through a treatment works using fluorescence spectroscopy. Environ. Technol. 34, 3069–3077.

Carvalho, L., Beber, J., De Souza, C.M., Geronazzo, M., Young, B.J., 2020. Phytotoxicity indexes and removal of color, COD, phenols and ISA from pulp and paper mill wastewater post-treated by UV/H2O2 and photo-Fenton. Ecotoxicol. Environ. Saf. 202, 110939.

Carvalho, S.I.M., Otero, M., Duarte, A.C., Santos, E.B.H., 2008. Effects of solar radiation on the fluorescence properties and molecular weight of fulvic acids from pulp mill effluents. Chemosphere 71, 1539–1546.

Cawley, K.M., Butler, K.D., Aiken, G.R., Larsen, L.G., Huntington, T.G., McKnight, D.M., 2012. Identifying fluorescent pulp mill effluent in the Gulf of Maine and its watershed. Mar. Pollut. Bull. 64, 1678–1687.

Chen, W., Westerhoff, P., Leenheer, J.A., Booksh, K., 2003. Fluorescence excitation-emission matrix regional integration to quantify spectra for dissolved organic matter. Environ. Sci. Technol. 37, 5701–5710.

Chen, W., Zhang, A., Jiang, G., Li, Q., 2019. Transformation and degradation mechanism of landfill leachates in a combined process of SAARB and ozonation. Waste Manag. 85, 283–294.

Cheng, C., Wu, J., You, L., Khan, M., 2018. Novel insights into variation of dissolved organic matter during textile wastewater treatment by fluorescence excitation-emission matrix. Chem. Eng. J. 335, 13–21.

Cheng, C., Liu, B., Liu, C., Shen, J., Wu, J., 2020. Tracking variation of fluorescent dissolved organic matter during full-scale printing and dyeing wastewater treatment. Chemosphere 252, 126559.

Cheng, S.Y., Show, P.L., Juan, J.C., Ling, T.C., 2021. Landfill leachate wastewater treatment to facilitate resource recovery by a coagulation-flocculation process via hydrogen bond. Chemosphere 262, 127829.
Chi, Z., Wang, Z., Liu, Y., Yang, G., 2018. Preparation of organosolv lignin-stabilized nano zero-valent iron and its application as granular electrode in the tertiary treatment of pulp and paper wastewater. Chem. Eng. J. 331, 317–325.
Chu, H., Wang, Z., Liu, Y., 2016. Application of modified bentonite granulated electrodes for advanced treatment of pulp and paper mill wastewater in three-dimensional electrode system. J. Environ. Chem. Eng. 1810–1817.
Ciputra, S., Antony, A., Phillips, R., Richardson, D., Leslie, G., 2010. Comparison of treatment options for removal of recalcitrant dissolved organic matter from paper mill effluent. Chemosphere 81, 86–91.
Cooper, J., Antony, A., Luiz, A., Leslie, G., 2019. Characterisation of dissolved organic matter in fermentation industry effluents and comparison with model compounds. Chemosphere 234, 630–639.
Da Silva, L.A., Flumignan, D.L., Tininis, A.G., Pezza, H.R., Pezza, L., 2019. Discrimination of brazilian lager beer by H NMR spectroscopy combined with chemometrics. Food Chem. 272, 488–493.
Dignac, M.F., Derenne, S., Largeau, C., 2000. Determination of structure and origin of refractory organic matter in bio-depurated wastewater via spectroscopic methods. comparison of conventional and ozonation treatments. Environ. Sci. Technol. 34, 3389–3394.
Duarte, R., Santos, E., Duarte, A., 2003. Spectroscopic characteristics of ultrafiltration fractions of fulvic and humic acids isolated from an eucalyptus bleached Kraft pulp mill effluent. Water Res. 37, 4073–4080.
Fagbemi, O.D., Sithole, B., Tesfaye, T., 2020. Optimization of keratin protein extraction from waste chicken feathers using hybrid pre-treatment techniques. Sustain. Chem. Pharm. 17, 100267.
Fan, H.J., Shu, H.Y., Yang, H.S., Chen, W.C., 2006. Characteristics of landfill leachates in Central Taiwan. Sci. Total Environ. 361, 25–37.
Fan, J., Li, H., Shuang, C., Li, W., Li, A., 2014. Dissolved organic matter removal using magnetic anion exchange resin treatment on biological effluent of textile dyeing wastewater. J. Environ. Sci. 26, 1567–1574.
Ferraz, F.M., Bruni, A.T., Povinelli, J., Vieira, E.M., 2016. Leachate/domestic wastewater aerobic co-treatment: a pilot-scale study using multivariate analysis. J. Environ. Manag. 166, 414–419.
Gong, X., Tian, W., Wang, L., Zhao, J., 2019. Biological regeneration of brewery spent diatomite and its reuse in basic dye and chromium(III) ions removal. Process Saf. Environ. Prot. 128, 353–361.
Gonsior, M., Zwartjes, M., Cooper, W.J., Song, W., Schmitt-Kopplin, P., 2011. Molecular characterization of effluent organic matter identified by ultrahigh resolution mass spectrometry. Water Res. 45, 2943–2953.
Goswami, L., Kumar, R.V., Pakshirajan, K., Pugazenthi, G., 2019. A novel integrated biodegradation—microfiltration system for sustainable wastewater treatment and energy recovery. J. Hazard. Mater. 365, 707–715.
Guleken, Z., Unubol, B., Bilici, R., Kuruca, S.E., 2020. Investigation of the discrimination and characterization of blood serum structure in patients with opioid use disorder using IR spectroscopy and PCA-LDA analysis. J. Pharm. Biomed. Anal. 190, 113553.
Guo, X., He, X., Zhang, H., Jiang, J., 2012. Characterization of dissolved organic matter extracted from fermentation effluent of swine manure slurry using spectroscopic techniques and parallel factor analysis (PARAFAC). Microchem. J. 102, 115–122.
He, X.S., Xi, B.D., Li, X., Cui, D.Y., 2013. Fluorescence excitation-emission matrix spectra coupled with parallel factor and regional integration analysis to characterize organic matter humification. Chemosphere 93, 2208–2215.
Huang, J., Fu, S., Gan, L., 2019. Lignin Chemistry and Applications. Elsevier ISBN: 9780128139417.
Hur, J., Lee, B.M., Choi, K.S., Min, B., 2014. Tracking the spectroscopic and chromatographic changes of algal derived organic matter in a microbial fuel cell. Environ. Sci. Pollut. Res. 21, 2230–2239.
Jaafarzadeh, N., Ghanbarri, F., Ahmadi, M., Omidinasab, M., 2017. Efficient integrated processes for pulp and paper wastewater treatment and phytotoxicity reduction: permanganate, electro-Fenton and Co3O4/UV/peroxymonosulfate. Chem. Eng. J. 308, 142–150.
Jain, R.M., Mody, K.H., Keshri, J., Jha, B., 2014. Biological neutralization and biosorption of dyes of alkaline textile industry wastewater. Mar. Pollut. Bull. 84, 83–89.
Janhom, T., Wattanachira, S., Pavasant, P., 2009. Characterization of brewery wastewater with spectrofluorometry analysis. J. Environ. Manag. 90, 1184–1190.
Jaria, G., Silva, C., Ferreira, C., Otero, M., Calisto, V., 2017. Sludge from paper mill effluent treatment as raw material to produce carbon adsorbents: an alternative waste management strategy. J. Environ. Manag. 188, 203–211.
Ji, F., Zhang, H., Li, J., Lai, B., 2017. Treatment of reverse osmosis (RO) concentrate from an old landfill site by Fe0/PS/O3 process. J. Chem. Technol. Biotechnol. 92, 2616–2625.
Jin, X., Zhang, W., Hou, R., Wang, X.C., 2019. Tracking the reactivity of ozonation towards effluent organic matters from WWTP using two-dimensional correlation spectra. J. Environ. Sci. 76, 289–298.
Kang, K.H., Shin, H.S., Park, H., 2002. Characterization of humic substances present in landfill leachates with different landfill ages and its implications. Water Res. 36, 4023–4032.
Karimipourfard, D., Eslamloueyan, R., Mehranbod, N., 2020. Heterogeneous degradation of stabilized landfill leachate using persulfate activation by CuFe2O4 nanocatalyst: an experimental investigation. J. Environ. Chem. Eng. 8, 103426.
Karthikeyan, S., Titus, A., Gnamani, A., Sekaran, G., 2011. Treatment of textile wastewater by homogeneous and heterogeneous Fenton oxidation processes. Desalination 281, 438–445.
Kaur, D., Bhardwaj, N., Lohchab, R., 2019. Effect of incorporation of ozone prior to ECF bleaching on pulp, paper and effluent quality. J. Environ. Manag. 236, 134–145.
Kumar, S., Gupta, N., Pakshirajan, K., 2015. Simultaneous lipid production and dairy wastewater treatment using rhodococcus opacus in a batch bioreactor for potential biodiesel application. J. Environ. Chem. Eng. 3, 1630–1636.
Lal, K., Garg, A., 2017. Utilization of dissolved iron as catalyst during Fenton-like oxidation of pretreated pulping effluent. Process Saf. Environ. Prot. 111, 766–774.
Lenz, S., Böhm, K., Ottner, R., Huber-Humer, M., 2016. Determination of leachate compounds relevant for landfill aftercare using FTIR spectroscopy. Waste Manag. 55, 321–329.
Li, W., Zhou, Q., Hua, T., 2010. Removal of organic matter from landfill leachate by advanced oxidation processes: a review. Int. J. Chem. Eng. 10, 270352.
Li, W., Xu, Z., Wu, Q., Li, Y., Shuang, C., Li, A., 2015. Characterization of fluorescent-dissolved organic matter and identification of specific fluorophores in textile effluents. Environ. Sci. Pollut. Res. 22, 4183–4189.
Li, Z., Yang, Q., Zhong, Y., Zeng, G., 2016. Granular activated carbon supported iron as a heterogeneous persulfate catalyst for the pretreatment of mature landfill leachate. RSC Adv. 6, 987.
Liu, B., Wu, J., Cheng, C., Shen, J., 2019. Identification of textile wastewater in water bodies by fluorescence excitation emission matrix – parallel factor analysis and high-performance size exclusión chromatography. Chemosphere 216, 617–623.
Liu, Z., Wu, W., Shi, P., Guo, J., Cheng, J., 2015. Characterization of Dissolved Organic Matter in Landfill Leachate During the Combined Treatment Process of Air Stripping, Fenton, SBR and Coagulation. 41, pp. 111–118.
Liu, Z., Li, X., Rao, Z., Hu, F., 2018. Treatment of landfill leachate biochemical effluent using the nano-Fe3O4/Na2S2O8 system: oxidation performance, wastewater spectral analysis and activator characterization. J. Environ. Manag. 208, 159–168.
Liu, Z., Pan, L., Hu, F., Hu, Y., 2020. Advanced landfill leachate biochemical effluent treatment using fe-Mn/AC activates O3/Na2S2O8 process optimization, wastewater quality analysis and activator characterization. Environ. Sci. Pollut. Res. 27, 15337–15349.
Louvet, J.N., Homeky, B., Casellas, M., Pons, M.N., Dagot, C., 2013. Monitoring of slaughterhouse wastewater biodegradation in a SBR using fluorescence and UV-visible absorbance. Chemosphere 91, 648–655.
Lu, F., Chang, C.H., Lee, D.J., Su, A., 2009. Dissolved organic matter with multi-peak fluorophores in landfill leachate. Chemosphere 74, 575–582.
Ma, C., He, Z., Jia, S., Zhang, X., Hou, S., 2018. Treatment of stabilized landfill leachate by Fenton-like process using Fe3O4 particles decorated zr-pillared bentonite. Ecotoxicol. Environ. Saf. 161, 489–496.
Ma, T., Wu, Y., Liu, N., Wu, Y., 2020. Hydrolized polyacrylamide modified diatomite waste as a novel adsorbent for organic dye removal: adsorption performance and mechanism studies. Polyhedron 175, 114227.
Ma, Y.B., Amamcharla, J.K., 2019. Front-face fluorescence spectroscopy combined with chemometrics to detect high proteinaceous matter in milk and whey ultrafiltration permeate. J. Dairy Sci. 102, 8756–8767.
Meenatchisundaram, S., Devaraj, M., Rai, C.L., Nadarajan, K.M., 2014. An integrated approach for enhanced textile dye degradation by pre-treatment combined biodegradation. Clean Techn. Environ. Policy 16, 501–511.
Mittal, G.S., 2006. Treatment of wastewater from abattoirs before land application – a review. Bioresour. Technol. 97, 1119–1135.
Moradi, S., Shayesteh, K., Behbudi, G., 2020. Preparation and characterization of biodegradable lignin-sulfonate nanoparticles using the microemulsion method to enhance the acetylation efficiency of lignin-sulfonate. Int. J. Biol. Macromol. 160, 632–641.
Muller, M., Marcondes, D., Déléris, S., Steyer, J.P., Dudal, Y., 2011. Solid-phase fluorescence spectroscopy to characterize organic wastes. Waste Manag. 31, 1916–1923.
Muniz, G.L., Borges, A.C., Fonseca da Silva, T.C., Oliveira, R., Ramos de Castro, S., 2020a. Chemically enhanced primary treatment of dairy wastewater using chitosan obtained from shrimp wastes: optimization using a doehlert matrix design. Environ. Technol. https://doi.org/10.1080/09593330.2020.1783372.
Muniz, G.L., Fonseca da Silva, T.C., Borges, A.C., 2020b. Assessment and optimization of the use of a novel natural coagulant (Guazuma ulmifolia) for dairy wastewater treatment. Sci. Total Environ. 744, 140854.
Navalon, S., Alvaro, M., García, H., 2011. Analysis or organic compounds in an urban wastewater treatment plant effluent. Environ. Technol. 32, 295–306.
Oloibiri, V., De Coninck, S., Chys, M.Van, Hulle, S.W.H., 2017. Characterisation of landfill leachate by EEM-PARAFAC-SOM during physical-chemical treatment by coagulation-flocculation, activated carbon adsorption and ion exchange. Chemosphere 186, 873–883.
Öncü-Kaya, E.M., Side, N., Özcam, A., 2017. Evaluation on dye removal capability of didodecyldimethylammonium-bentonite from aqueous solution. J. Dispers. Sci. Technol. 38, 1211–1220.
Outeiriño, D., Costa-Trigo, I., Paz, A., Deive, F.J., Rodríguez, A., Domínguez, J.M., 2019. Biorefining brewery spent grain polysaccharides trough biotuning of ionic liquids. Carbohydr. Polym. 203 (265), 274.
Pernet-Coudrier, B., Clouzot, L., Varrault, G., Mouchel, J.M., 2008. Dissolved organic matter from treated effluent of a major wastewater treatment plant: characterization and influence on copper toxicity. Chemosphere 73, 593–599.
Pretsch, E., Bühlmann, P., Badertscher, M., 2009. Structure Determination of Organic Compounds: Tables of Spectral Data. Springer ISBN: 978-3-540-93809-5.
Rabinovich, A., Rouff, A., Lew, B., Ramlogan, M., 2018. Aerated fluidized bed treatment for phosphate recovery from dairy and swine wastewater. Sustain. Chem. Eng. 6, 652–659.
Renou, S., Givaudan, J.G., Poulain, S., Moulin, P., 2008. Landfill leachate treatment: review and opportunity. J. Hazard. Mater. 150, 468–493.
Rodríguez, F., Schlenger, P., García-Valverde, M., 2016. Monitoring changes in the structure and properties of humic substances following ozonation using UV-vis, FTIR and 1H NMR techniques. Sci. Total Environ. 541, 623–637.
Rodríguez-Vidal, F.J., García-Valverde, M., Ortega-Azabache, B., González-Martínez, A., Bellido-Fernández, A., 2020. Characterization of urban and industrial wastewaters

using excitation-emission matrix (EEM) fluorescence: searching for specific fingerprints. J. Environ. Manag. 263, 110396.
Sales, J.O., Dos Santos, M.V., Morais, C., Pegado, R., 2020. Spectrochemical analysis in blood plasma combined with subsequent chemometrics for fibromialgia detection. Sci. Rep. 10, 11769.
Santos, E.B.H., Filipe, O.M.S., Duarte, R.M.B.O., Pinto, H., Duarte, A.C., 2000. Fluorescence as a tool for tracing the organic contamination from pulp mill effluents in surface waters. Acta Hydrochim. Hydrobiol. 28, 364–371.
Santos, P.S.M., Otero, M., Duarte, R.M.B.O., Duarte, A.C., 2009. Spectroscopic characterization of dissolved organic matter isolated from rainwater. Chemosphere 74, 1053–1061.
Senn, H., Cusanovich, M., Würthrich, K., 1984. H NMR assignments for the heme group and electronic structure in chlorobium thiosulfatophilum cytochrome c-555. Biochim. Biophys. Acta 785, 46–53.
Sethupathy, A., Sivashanmugam, P., 2018. Enhancing biomethane potential of pulp and paper sludge through disperser mediated polyhydroxyalkanoates. Energy Convers. Manag. 173, 179–186.
Sharma, A., Syed, Z., Ram, C., 2019. Adsorption of textile wastewater on alkali-activated sand. J. Clean. Prod. 220, 23–32.
Shouliang, H., Beidou, X., Haichan, Y., Liansheng, H., Shilei, F., Hongliang, L., 2008. Characteristics of dissolved organic matter (DOM) in leachate with different landfill ages. J. Environ. Sci. 20, 492–498.
Shumilina, E., Johansen, T., Glasner, C.R., Dikiy, A., 2020. Application of NMR spectroscopy and conventional analytical methods for the assessment of wastewater from food industry. Waste Biomass Valoriz. 11, 1349–1357.
Silbir, S., Goksongur, Y., 2019. Natural red pigment production by monascus purpureus in submerged fermentation systems using a food industry waste: Brewer's spent grain. Foods 8, 161.
Silva, M.E., Santos, M., Brás, I., 2019. Characterization of wastewater from landfills-amount and type of humic substances extracted from leachate. E3S Web Conf. 80, 03002.
Simpson, A.J., Lefebvre, B., Moser, A.M., Kelleher, B., 2004. Identifying residues in natural organic matter through spectral prediction and pattern matching of 2D NMR datasets. Magn. Reson. Chem. 42, 14–22.
Smidt, E., Meissl, K., 2007. The applicability of fourier transform infrared (FT-IR) spectroscopy in waste management. Waste Manag. 27, 268–276.
Sonkar, M., Kumar, M., Dutt, S., Kumar, V., 2019. Treatment of pulp and paper mill effluent by a novel bacterium bacillus sp. IITRDVM-5 through a sequential batch process. Biocat. Agric. Biotechnol. 20, 101232.
Stafussa, A.P., Maciel, G.M., Da Silva, A.G., Haminiuk, C.W.I., 2016. Biosorption of anthocyanins from grape pomace extracts by waste yeast: kinetic and isotherm studies. J. Food Eng. 169, 53–60.
Sudarshan, K., Maruthaiya, K., Kotteswaran, P., Murugan, A., 2016. Reduction of pollutants in hardwood pulp mill bleach effluent. Asian J. Chem. 28 (12), 2641–2644.
Sun, W., Yue, D., Song, J., Nie, Y., 2018. Adsorption removal of refractory organic matter in bio-treated solid waste landfill leachate by anion exchange resins. Waste Manag. 81, 61–70.
Tahiri, A., Richel, A., Destain, J., Ongena, M., 2016. Comprehensive comparison of the chemical and structural characterization of landfill leachate and leonardite humic fractions. Anal. Bioanal. Chem. 408, 1917–1928.
Tonk, S., Nagy, B., Török, A., Indolean, C., Majdik, C., 2015. Cd (II), zn (II) and cu (II) bioadsorption on chemically treated waste brewery yeast biomass: the role of functional groups. Acta Chim. Slov. 62, 736–746.
Upadhyay, D., Singh, A., Das, P., Sharma, U., 2020. Abnormalities in metabolic pathways in celiac disease investigated by metabolic profiling of small intestinal mucosa, blood plasma and urine by NMR spectroscopy. NMR Biomed. 33 (8), 1–19.
Wang, F., Luo, Y., Ran, G., Li, Q., 2020. Sequential coagulation and Fe0-O3/H2O2 process for removing recalcitrant organics from semi-aerobic aged refuse biofilter leachate: treatment efficiency and degradation mechanism. Sci. Total Environ. 699, 134371.
Wang, H.W., Li, X.Y., Hao, Z.P., Tsang, Y.F., 2017. Transformation of dissolved organic matter in concentrated leachate from nanofiltration during ozone-based oxidation processes (O3, O3/H2O2 and O3/UV). J. Environ. Manag. 191, 244–251.
Wang, L., Yang, Q., Wang, D., Yi, K., 2016. Advanced landfill leachate treatment using iron-carbon microelectrolysis-Fenton process: process optimization and column experiments. J. Hazard. Mater. 318, 460–467.
Wang, W.L., Cai, Y.Z., Hu, H.Y., Wu, Q.Y., 2019. Advanced treatment of bio-treated dyeing and finishing wastewater using ozone-biological activated carbon: a study on the synergistic effects. Chem. Eng. J. 359, 168–175.
Weathers, L.J., 1995. Industrial wastes: fermentation industry. Water Environ. Res. 67, 517–522.
Wöjtowicz, H., Wojaczyñnski, J., Olczak, T., 2009. Heme environment in HmuY, the heme-binding protein of porphyromonas gingivalis. Biochem. Biophys. Res. Comm. 383, 178–182.
Wu, Q., Li, W.T., Yu, W.H., Li, Y., Li, A.M., 2016. Removal of fluorescent dissolved organic matter in biologically treated textile wastewater by ozonation-biological aerated filter. J. Taiwan Inst. Chem. Eng. 59, 359–364.
Xi, B.D., Wei, Z.M., Zhao, Y., Yang, T.X., 2008. Study on fluorescence characteristic of dissolved organic matter from municipal solid waste landfill leachate. Spectrosc. Spectr. Anal. 28, 2605–2608.
Xiaoli, C., Yongxia, H., Guixiang, L., Youcai, Z., 2013. Spectroscopic studies of the effect of aerobic conditions on the chemical characteristics of humic acid in landfill leachate and its implication for the environment. Chemosphere 91, 1058–1063.
Xu, Y., Zhang, L., Pan, Y., Qian, G., 2017. Utilization of calcium-based and aluminum-based materials for the treatment of stabilized landfill leachate: a comparative study. Environ. Sci. Pollut. Res. 24, 26821–26828.
Yang, L., Han, D.H., Lee, B.M., Hur, J., 2015. Characterizing treated wastewaters of different industries using clustered fluorescence EEM-PARAFAC and FTIR spectroscopy: implications for downstream impact and source identification. Chemosphere 127, 223–228.
Yin, Z., Yang, C., Long, C., Li, A., 2017. Influence of surface properties of RO on membrane fouling for treating textile secondary effluent. Environ. Sci. Pollut. Res. 24, 16253–16262.
Yin, Z., Yang, C., Long, C., Li, A., 2018. Effect of integrated pretreatment technologies on RO membrane fouling for treating textile secondary effluent: Laboratory and pilot-scale experiments. Chem. Eng. J. 332, 109–117.
Yurtsever, A., Calimlioglu, B., Görur, M., Çinar, O., Sahinkaya, E., 2016. Effect of NaCl concentration on the performance of sequential anaerobic and aerobic membrane bioreactors treating textile wastewater. Chem. Eng. J. 287, 456–465.
Zegzouti, Y., Boutafda, A., Ezzariai, A., Hafidi, M., 2020. Bioremediation of Landfill Leachate by Aspergillus flavus in Submerged Culture: Evaluation of the Process Efficiency by Physicochemical Methods and 3D Fluorescence Spectroscopy. 225, p. 109821.
Zhang, Q.Q., Tian, B.H., Zhang, X., Ghulam, A., Fang, C.R., He, R., 2013. Investigation on characteristics of leachate and concentrated leachate in three landfill leachate treatment plants. Waste Manag. 33, 2277–2286.
Zheng, X., Khan, M.T., Croué, J.P., 2014. Contribution of effluent organic matter (EfOM) to ultrafiltration (UF) membrane fouling: isolation, characterization and fouling effect of EfOM fractions. Water Res. 65, 414–424.
Zhu, W., Westman, G., Theliander, H., 2015. The molecular properties and carbohydrate content of lignins precipitated from black liquor. Holzforschüng 69, 143–152.
Zinadini, S., Vatanpour, V., Zinatizadeh, A., Kian, M., 2015. Preparation and characterization of antifouling graphene oxide/polyethersulfone ultrafiltration membrane: application in MBR for dairy wastewater treatment. J. Water Process Eng. 7, 250–254.